atmosphere

MDPI

Article

Analyzing the Influence of Vehicular Traffic on the Concentration of Pollutants in the City of São Paulo: An Approach Based on Pandemic SARS-CoV-2 Data and Deep Learning

Gregori de Arruda Moreira [1,2,*], Alexandre Cacheffo [2,3], Izabel da Silva Andrade [2], Fábio Juliano da Silva Lopes [2,4], Antonio Arleques Gomes [2] and Eduardo Landulfo [2]

1 Federal Institute of São Paulo (IFSP), Campus Registro, São Paulo 11900-000, Brazil
2 Center for Lasers and Applications (CELAP), Institute of Energy and Nuclear Research (IPEN), São Paulo 05508-000, Brazil; cacheffo@ufu.br (A.C.); izabel.andrade@usp.br (I.d.S.A.); fabiolopes@alumni.usp.br (F.J.d.S.L.); antonio.gomes@usp.br (A.A.G.); elandulf@ipen.br (E.L.)
3 Institute of Exact and Natural Sciences of Pontal (ICENP), Federal University of Uberlândia (UFU), Campus Pontal, Ituiutaba 38304-402, Brazil
4 Department of Environmental Sciences, Institute of Environmental, Chemical and Pharmaceutical Sciences (ICAQF), Federal University of São Paulo (UNIFESP), Campus Diadema, São Paulo 09913-030, Brazil
* Correspondence: gregori.moreira@ifsp.edu.br

Abstract: This study employs surface and remote sensing data jointly with deep learning techniques to examine the influence of vehicular traffic in the seasonal patterns of CO, NO_2, $PM_{2.5}$, and PM_{10} concentrations in the São Paulo municipality, as the period of physical distancing (March 2020 to December 2021), due to SARS-CoV-2 pandemic and the resumption of activities, made it possible to observe significant variations in the flow of vehicles in the city of São Paulo. Firstly, an analysis of the planetary boundary layer height and ventilation coefficient was performed to identify the seasons' patterns of pollution dispersion. Then, the variations (from 2018 to 2021) of the seasonal average values of air temperature, relative humidity, precipitation, and thermal inversion occurrence/position were compared to identify possible variations in the patterns of such variables that would justify (or deny) the occurrence of more favorable conditions for pollutants dispersion. However, no significant variations were found. Finally, the seasonal average concentrations of the previously mentioned pollutants were compared from 2018 to 2021, and the daily concentrations observed during the pandemic period were compared with a model based on an artificial neural network. Regarding the concentration of pollutants, the primarily sourced from vehicular traffic (CO and NO_2) exhibited substantial variations, demonstrating an inverse relationship with the rate of social distancing. In addition, the measured concentrations deviated from the predictive model during periods of significant social isolation. Conversely, pollutants that were not primarily linked to vehicular sources ($PM_{2.5}$ and PM_{10}) exhibited minimal variation from 2018 to 2021; thus, their measured concentration remained consistent with the prediction model.

Keywords: COVID-19; remote sensing; machine learning; pollutants

Citation: Moreira, G.d.A.; Cacheffo, A.; Andrade, I.d.S.; Lopes, F.J.d.S.; Gomes, A.A.; Landulfo, E. Analyzing the Influence of Vehicular Traffic on the Concentration of Pollutants in the City of São Paulo: An Approach Based on Pandemic SARS-CoV-2 Data and Deep Learning. *Atmosphere* **2023**, *14*, 1578. https://doi.org/10.3390/atmos14101578

Received: 28 September 2023
Revised: 14 October 2023
Accepted: 17 October 2023
Published: 19 October 2023

1. Introduction

Among many problems affecting big urban centers worldwide, atmospheric pollution is among the most critical [1]. During the last decades, several studies [1–3] have addressed the harmful effects that this type of pollution causes, mainly on human health. However, understanding the emission and dispersion processes of pollutants and quantifying the role of each emission source is not easy, given the complex scenario of large cities, where several sources act simultaneously.

In early 2020, due to the rapid spread of the new coronavirus SARS-CoV-2, governments worldwide created unprecedented social distancing policies to mitigate the evolution of population contamination rates. Such measures restricted the execution of several activities that were classified as non-essential, resulting in a considerable reduction in vehicular traffic and industrial activities considering that it directly impacted dynamic measurements in the urban environment on seismic noise [4], urban sound [5], light pollution [6], and, especially, air quality [7]. In addition, it is important to highlight that this situation created the possibility of deeply analyzing the relationship between the decrease in emission rates from the specific anthropogenic sources and the variations in the concentration of the pollutants [3].

When performing a comparison between the period prior to lockdown and the lockdown period, a reduction in the concentration of NO_2 was observed in Brazil [8,9], China [10], Ecuador [11], India [12], Italy [13], Morocco [14], Spain [15], and in the USA [16]. Also, a significant reduction in CO concentration was observed in Brazil [8,9], China [10], Ecuador [11], India [12], and Italy [13]. On the other hand, some pollutants, such as particulate matter (PM) and O_3, did not show significant reduction rates; therefore, some studies [9,15,16] reported increased concentrations during the lockdown period. Such results, specifically for $PM_{2.5}$, may be related to its complex non-linear atmospheric formation process [3] and biomass-burning activities [9]. A deep review of the influence of COVID-19 on the pollutant concentrations in urban regions can be found in [7].

Nevertheless, considering that after the start of vaccinations and, consequently, a reduction in contagion rates, several countries began resuming economic activities in May 2020, which generated questions such as: How quickly did pollutant concentrations return to pre-pandemic levels? Were all pollutants affected in the same way? Which physical distancing levels significantly affect pollutant concentrations?

São Paulo, the most populous city in South America (around 12.8 million inhabitants, which represents approximately 6% percent of Brazil's population) [17], has an extensive vehicle fleet (approximately 9.1 million). This fleet acts as a significant source of anthropogenic pollutants such as PM_{10} (40%), $PM_{2.5}$ (37%), CO (97%), NO_X (64%), SO_X (17%), and hydrocarbons (76%) [18,19]. Between March and May, São Paulo's State Government decreed a partial lockdown, which caused a physical distancing rate in the city of São Paulo of around 55% [20]. Such action caused a reduction in vehicle circulation of 86% during the more restrictive period [20]; thus, some studies [21,22] presented results related to reducing some pollutants in this period. In comparison with the results of the previous months, Siciliano et al. [21] showed air quality data from the Companhia Ambiental do Estado de São Paulo (CETESB) at the beginning of the partial lockdown (23 March 2020 to 3 April 2020) that identified a significant reduction in the concentrations of NO_2 (14.5% to 32.9%), CO (33.0% to 40.0%), and PM_{10} (2.8% to 10.0%) in the city of São Paulo. Nakada and Urban [22], using data from the Tropospheric Monitoring Instrument (TROPOMI) onboard the Sentinel-5P satellite, also identified a reduction in the concentration of NO_2 (54.3%) and CO (64.8%) between March and April 2020 in comparison with the same period of the previous year in the city of São Paulo.

However, due to the creation of the "Plano São Paulo" (https://www.saopaulo.sp.gov.br/planosp/ (accessed on 1 January 2022)) by the São Paulo municipality, the resumption of economic activities began on 1 June 2020, which caused a gradual decrease in the physical distancing rate and consequently an increase in the vehicle traffic.

In order to demonstrate the role of vehicular traffic in the concentration of CO, NO_2, $PM_{2.5}$, and PM_{10} in the city of São Paulo, this paper presents a comparison among the seasonal variation of such pollutants in the period before (2018 to 2019), during (March to June 2020), and after (July 2020 to December 2021) the partial lockdown. Firstly, from remote sensing data, a description of the seasonal behavior of the planetary boundary layer height and the ventilation coefficient will be presented to demonstrate that such variables can affect the patterns of pollutant dispersions in the city of São Paulo. Then, a comparison among the values of air surface temperature, relative humidity, precipitation,

and thermal inversion occurrence from 2018 to 2021 will be performed to try to identify the incidence, or deny it, of events that justify any variations in the pollutant concentrations. Finally, a comparison of the concentrations of the previously mentioned pollutants from 2018 to 2021 will be performed to identify how the variation of the physical distancing influenced the concentration of such pollutants. In addition, to improve the comparison, an Artificial Neural Network (ANN) was trained to predict the pollutant concentrations in non-pandemic situations, and the results were compared with those measured from March 2020 to December 2021, where the physical distancing rate had significative variations.

This paper will have the following structure: Section 2 will briefly describe the experimental site and instruments. In Section 3, the methodology will be described. The results and discussions will be presented in Sections 4 and 5, respectively. Finally, the conclusions will be presented in Section 6.

2. Experimental Site and Instrumentation

2.1. São Paulo

The city of São Paulo is located in the southeastern region of Brazil, where the humid subtropical climate predominates [autumn (March, April, and May), winter (June, July, and August), spring (September, October, and November), summer (December, January, and February), in general, with a hot and humid summer and a dry winter period. Average temperatures in winter are lower than those in the summer, but the difference is not as pronounced. Spring and autumn have a milder intermediate climate, although there is much rainfall in early autumn [23,24].

All of the data presented in the following sub-sections were obtained from 2018 to 2021. Within this period, the care regime adopted concerning the pandemic (social distancing, the closing of commerce, the closing of schools and universities, and the reduction in the flow of vehicles and public transport, among other protocols) occurred more pronouncedly between March and May 2020. The subsequent resumption of economic activities, organized through the "Plano São Paulo" (Sao Paulo Plan [25]), began in June 2020 and continued maintaining some activity restrictions throughout 2021. Consequently, the instruments that could not be operated remotely (Lidar system and radiosonde launching) did not work from March 2020 to December 2021 due to the COVID-19 pandemic. Throughout this work, 2018 and 2019 will be addressed as the pre-pandemic period, while 2020 and 2021 will be the pandemic period.

2.1.1. CETESB Stations

The data were collected from four CETESB stations in São Paulo: Pinheiros, Parque Dom Pedro II, Ponte dos Remédios, and Congonhas. They were selected because, besides providing information about CO, NO_2, $PM_{2.5}$, and PM_{10}, they belong to four important regions of São Paulo, making them highly representative for the study proposed in this paper. Their locations are shown in Figure 1. The Congonhas Station (23°36′ S, 46°39′ W), near the airport of the same name (the second busiest airport in Brazil, with an average of 21 million passengers per year), is located in a region of the city with heavy vehicle traffic (North–South Corridor and Bandeirantes Avenue). The Parque Dom Pedro II Station (23°32′ S, 46°37′ W) is located in the historic center of the city (near Avenida do Estado, a corridor with heavy vehicle traffic). The Pinheiros (23°33′ S, 46°37′ W) Station, located in the western region of the city, is close to Marginal Pinheiros (part of the SP-15 highway), a road with an intense movement of light and heavy vehicles, which is the second busiest in the city. Finally, Ponte dos Remédios Station (23°31′ S, 46°44′ W) is located in the northern region of the town, next to Marginal Tietê (another part of the SP-15 highway), which is the busiest road in the city (and in Brazil), through which about 1.2 million vehicles pass per day [24].

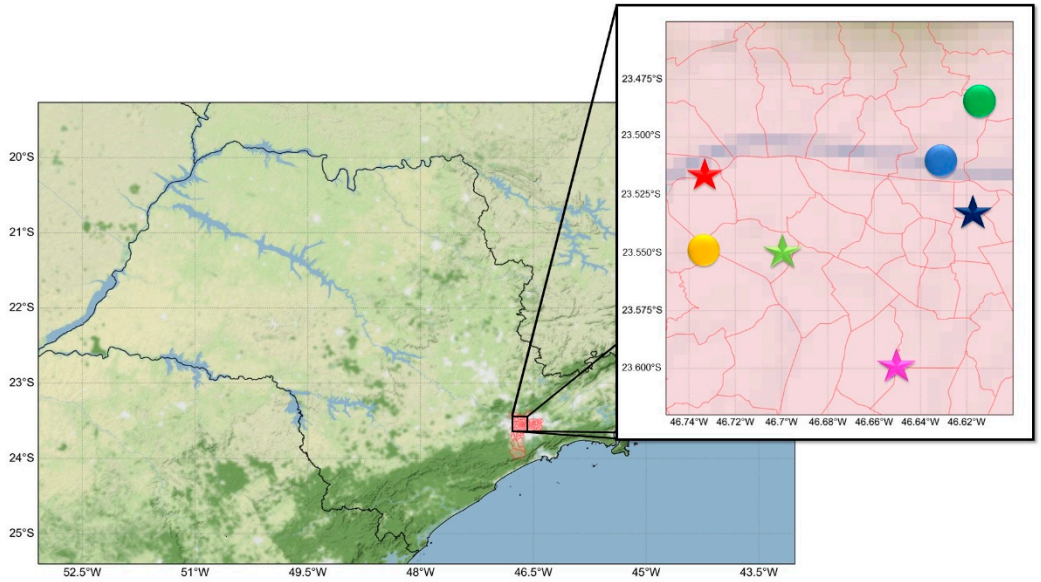

Figure 1. São Paulo municipality map. The red, light green, dark blue, and pink stars represent the four CETESB stations addressed in this paper (Ponte dos Remédios, Pinheiros, Parque Dom Pedro II, and Congonhas). The yellow, green, and blue circles represent the location of the SPU Lidar Station, Mirante de Santana Station, and Campo de Marte Airport, respectively.

2.1.2. SPU Lidar Station

The Lidar Station SPU (Figure 1) is installed at the Lasers and Applications Center (23°33′ S, 46°44′ W) of the Institute for Energy and Nuclear Research (CELAP/IPEN). The station has monitored aerosols' optical properties and vertical distribution for approximately 20 years. The Lidar system operates in the coaxial mode, using a pulsed Nd: YAG laser, emitting radiation at 355 nm, 532 nm, and 1064 nm to the zenith, with a repetition rate of 10 Hz. Three elastic channels (355, 532, and 1064 nm) and three Raman channels (387, 408, and 530 nm) detect the received signal. The measurements obtained from the lidar and used in this work correspond to a wavelength of 532 nm (elastic). The temporal resolution adopted is 1 min, and the spatial resolution is 7.5 m. Complete overlap is achieved at an altitude of 300 m, a.g.l. [26].

2.1.3. Rainfall Rate and Vertical Temperature Profile

The rainfall data were obtained from Mirante de Santana station (23°29′ S, 46°37′ W) (Figure 1). This station and countless others spread throughout the Brazilian territory are maintained and operated by the National Institute of Meteorology (Inmet) [27]. The thermal inversions were estimated from the vertical temperature profiles provided by the radiosondes launched at the Campo de Marte Airport (23°30′ S, 46°38′ W) (Figure 1) at 09:00 LT (daily).

2.1.4. CETESB QUALAR Platform

São Paulo has an overall monitoring air quality system, with automatic and manual stations all over its territorial extension. Among all the cities in this state, the capital, São Paulo municipality, has the most significant number of stations. The data acquired and recorded by these stations are available to download on the CETESB's QUALAR platform [28]. Such a platform allows the public access to the data obtained by the stations, the air quality indexes in real time, specific reports (daily values of pollutants, monthly mean, distribution of air quality, and others), and filters to export the data (such as the station, variables, and interest time).

The data retrieved from the QUALAR for the analyses were the concentrations of NO_2, CO, $PM_{2.5}$, and PM_{10}, with a temporal resolution of 1 h, for the following stations of

CETESB: Pinheiros, Parque Dom Pedro II, Ponte dos Remédios, and Congonhas (Figure 1). In addition, the collected data from the Pinheiros Station comprised surface relative humidity, surface temperature, horizontal wind speed (HWS), with a temporal resolution of 1 h, and the daily number of occurrences of thermal inversions, as well as the heights at which they occur. All analyses presented in Section 4 are based on the average of these four stations.

3. Theory and Methods

3.1. Atmospheric Boundary Layer Height

The atmospheric boundary layer (ABL) is the lowermost region of the troposphere "*that is directly influenced by the presence of the earth's surface and responds to surface forcing within a timescale of about an hour or less*" [29]. This layer has mechanical and thermodynamic turbulent characteristics, which play a fundamental role in the dispersion of pollutants.

During its daily cycle, the ABL has height variations, which are directly associated with the stability of this layer. At the beginning of the day, the heat transfer process initiates as the ground becomes warm, and convective thermals cause turbulent mixing. Such a phenomenon gives rise to the ABL sublayer denominated convective boundary layer (CBL), which grows throughout the day. After sunset, due to the radiative cooling of the ground, the turbulence mixing is suppressed and CBL is substituted by a shallow stable sublayer, named the stable boundary layer (SBL). A sublayer covers the SBL (with intermittent turbulence, not affected by the turbulence transport from the surface), and is denominated as the residual layer (RL). RL has the same height as the maximum reached by the CBL on the previous day [29]. Due to high-ABLH variability, remote sensing instruments endowed with high-temporal resolution (e.g., elastic lidar) are widely applied in analyzing the ABLH's daily cycle.

ABLH Daily Cycle from Elastic Lidar Data

Due to the overlap of the SPU Lidar, the lidar measurements were carried out from 10:00 to 18:00 local time (LT) to provide estimates of the CBL height (CBLH).

All lidar results were obtained from the raw signal (P) with a wavelength of 532 nm, which was pre-processed with a three-step correction (dark current [DC] remotion, background radiation [BG] remotion, correction with the square of the height [z^2]) described in Refs. [30,31]. After this, the range corrected signal (RCS_{532}) is obtained, as indicated in the equation below.

$$RCS_{532}(z) = (P(z) - DC(z) - BG)z^2, \quad (1)$$

Then, from the RCS_{532}, the CBLH was detected using the wavelet covariance transform method (WCT) [30]. Such a method performs a covariance (W(a, b)) between a mother wavelet (Haar function [h]) and the average RCS_{532} obtained in one hour ($\overline{RCS}_{532}$) as follows:

$$W(a,\ b) = \frac{1}{a}\int_{z_i}^{z_f} \overline{RCS}_{532}(z)h\left(\frac{z-b}{a}\right)dz, \quad (2)$$

where a and b are the values of dilatation and transition related to the mother wavelet, z_i and z_f are the respective lower and upper limits of the CBL, and z is the height above the ground. This method identifies the CBLH at the height where the transition between the ABL and the free troposphere occurs, characterized by the high reduction in aerosol concentration. In other words, CBLH is the maximum in the covariance profile as shown below.

$$CBLH = Max(W(a, b)), \quad (3)$$

3.2. Ventilation Coefficient

The ventilation coefficient (VC) is an important parameter to evaluate the dispersion of pollutants in the CBL region. It represents the rate at which air is transported away from a particular area. The VC is obtained as indicated in the following equation [9]:

$$VC = CBLH\overline{HWS}, \quad (4)$$

where $\overline{HWS}$ is the one-hour average of the horizontal wind speed.

3.3. Thermal Inversions

Thermal inversions (TIs) are a recurrent phenomenon in São Paulo, mainly during winter [14]. The TIs can attenuate the convective process, inhibiting the dispersions process and confining the pollutants in the region below it. Evaluating such a phenomenon can interfere with pollutant concentration from the temperature profiles provided by the radiosondes (launched at 09:00 LT) data. On these heights, TIs were identified and classified into three groups: below 200 m, between 200 m and 500 m, and above 500 m.

3.4. Prediction of Pollutant Concentrations

An Artificial Neural Network (ANN) algorithm (NeuralProphet) [32] was applied to estimate the expected concentration of each analyzed pollutant in non-pandemic situations in 2020 and 2021. Such a Python library combines neural network techniques and time-series regression algorithms to provide forecasts. As the input, the daily average concentration of each pollutant (CO, NO_2, $PM_{2.5}$, and PM_{10}) was used in the four analyzed CETESB stations from 2018 to 2019. A total of 70% of this data was applied in the training stage, and 30% was used to test the model. Thus, mean absolute error values of 0.14 ppm, 10.8 $\mu g \cdot m^{-3}$, 4.1 $\mu g \cdot m^{-3}$, and 7.1 $\mu g \cdot m^{-3}$ to CO, NO_2, $PM_{2.5}$, and PM_{10} were obtained, respectively. This method allowed us to compare the variation of pollutant concentrations during the pandemic.

4. Results and Discussion

4.1. Analysis of Meteorological Variables

4.1.1. The PBLH and VC

The PBLH presents a similar behavior during all seasons (Figure 2), where the lower values occur between 14 and 15 UTC (due to the low convection activity), the growth stage starts between 15 and 16 UTC, and the maximum height is reached between 18 and 19 UTC, which corresponds to middle afternoon at which point the convective boundary layer is already well-mixed. Regarding the seasonal behavior, the higher average PBLH occurs in summer (Figure 2d) ((1690 $\pm$ 220) m at 19 UTC) due to higher radiation capture and, consequently, intense convective activity [31]. Lower levels are observed during the winter ((750 $\pm$ 160) m at 21 UTC) (Figure 2b), which is caused by the lower radiation capture, resulting in low convective activity in comparison to other seasons. Although VC also has a daily cycle (Figure 2) with a behavior similar to the PBLH (lowest values around 14 UTC and maximum values between 18 and 19 UTC), it decreases during the late afternoon due to a reduction in $\overline{HWS}$. In addition, VC has a seasonal behavior, where the higher average values occur in summer (mainly at 19 UTC, where VC reaches (3700 $\pm$ 910) m^2/s) (Figure 2d). The lower levels are concentrated in autumn (Figure 2a) and winter (mainly at 21 UTC where VC reaches (1310 $\pm$ 260) m^2/s).

Therefore, considering the influence of PBLH and VC in the pollutants' dispersion process [31], the lower concentrations tend to be observed during the summer (highest values of PBLH and VC), while the higher ones tend to occur during the winter. On the other hand, spring and autumn present intermediate levels.

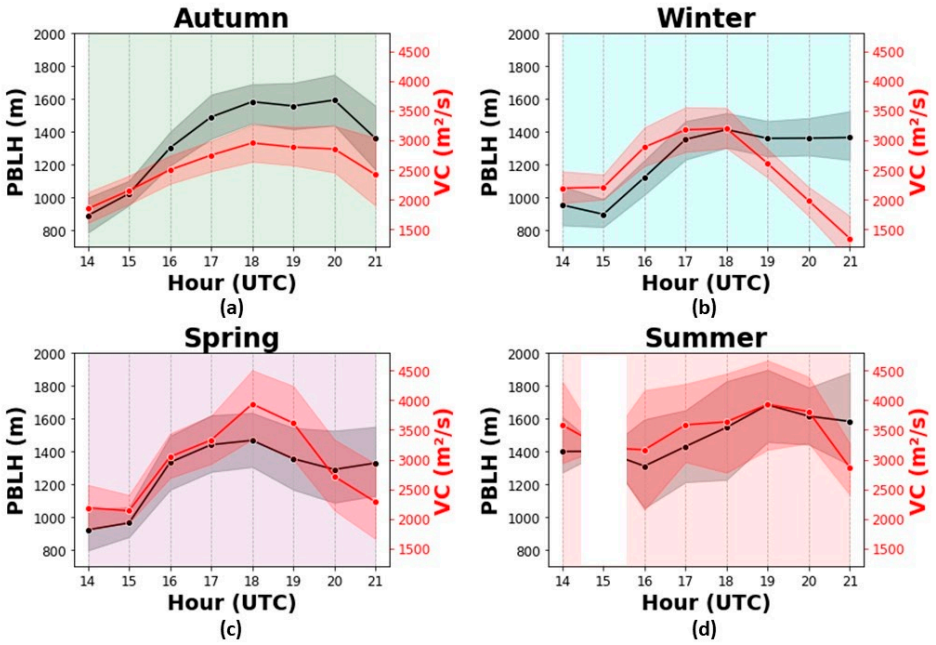

Figure 2. Seasonal ((**a**) Autumn, (**b**) Winter, (**c**) Spring, and (**d**) Summer) variation of PBLH (black lines) and VC (red lines) from 2018 to 2019. There are no lidar measurements at 15 UTC during summer due to solar radiation incidence.

4.1.2. Thermal Inversions

Table 1 presents the number of TIs per season from 2018 to 2021. Considering the total TI, the higher occurrence is always in the winter for all of the analyzed years, as expected [18]. From 2018 to 2019, 538 TIs were detected; between 2020 and 2021, 558 TIs were registered. All years follow a similar pattern, with a small occurrence of TIs in the region below 200 m and a high one above 500 m; hence, this region is situated over the PBL top. Afterwards, TIs inhibit the growth of this layer, causing an increase in the pollutants' concentration in the lower troposphere region.

Table 1. Number of thermal inversions in city of São Paulo from 2018 to 2021. The smallest occurrences tend to be yellow, while the largest tend to be brown.

Seasons	<200m				200–500 m				>500 m			
	2018	2019	2020	2021	2018	2019	2020	2021	2018	2019	2020	2021
summer	4	13	0	0	16	15	14	14	45	26	44	45
autumn	5	5	6	9	31	24	28	29	34	34	49	36
winter	22	12	17	20	28	25	30	29	33	23	35	36
spring	3	4	4	1	23	21	20	26	42	50	25	41

4.1.3. Air Surface Temperature, Relative Humidity, and Precipitation

Figure 3 presents the seasonal variations of surface temperature (Figure 2a), relative humidity (Figure 2b), and accumulated precipitation (Figure 2c) from 2018 to 2021. During all analyzed periods, summer and winter remain the hottest and coldest seasons (Figure 2a), respectively, as expected. From the four analyzed years, 2019 is characterized by the hottest summers ((23.6 $\pm$ 1.4) °C) and the coldest winter ((18.0 $\pm$ 1.0) °C). Regarding relative humidity (Figure 2b), except in 2019, the lower average values are consistently observed in winter. Summers of 2020 and 2021 had a wet season ((72.9 $\pm$ 3.7)% and (70.5 $\pm$ 0.9)%, respectively), while in 2018 and 2019, the higher values of relative humidity can be observed in spring ((72.3 $\pm$ 3.5)%) and autumn ((71.1 $\pm$ 2.2)%), respectively. As expected, the higher values of accumulated precipitation for the four analyzed years were observed during the

summer, mainly in 2020 (1046 mm) (Figure 2c). Excluding 2020, where the lowest values occurred in autumn (87.8 mm), the lowest accumulated precipitation rates were consistently observed in winter (86.6, 192.4, and 97.0 mm in 2018, 2019, and 2021, respectively).

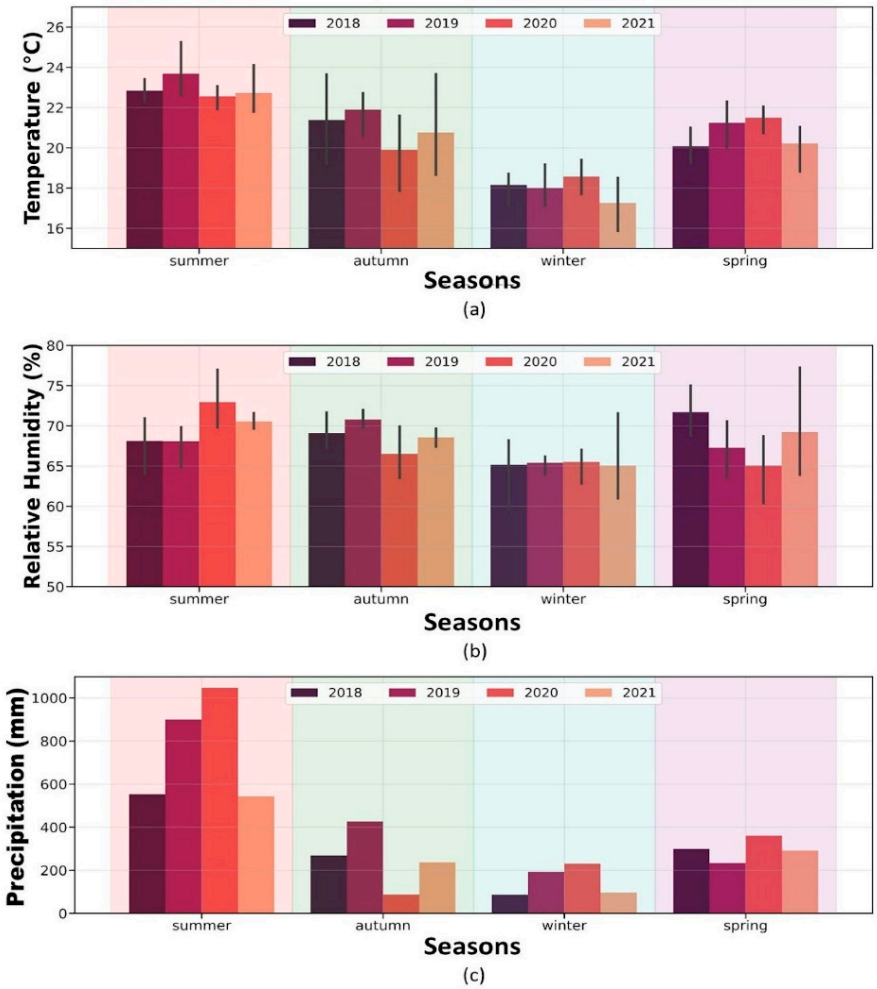

Figure 3. Seasonal variation of (**a**) mean surface temperature, (**b**) mean surface relative humidity, and (**c**) accumulated precipitation from 2018 to 2021.

Therefore, for all of the analyzed years, it is possible to observe a seasonal pattern where the summer and winter seasons have more outstanding characteristics than the other seasons. While the summers are endowed with a higher temperature, relativity humidity, accumulated precipitation rates, VC, and PBLH values, the winters have a lower temperature, relativity humidity, accumulated precipitation rates, PBLH, and a high number of TI. Considering the behavior of the seasons over the years, none of the analyzed variables presented any abrupt variation that would justify the intensification or attenuation in the process of dispersion of pollutants. Therefore, it is reasonable to assume that any variation in the pollutants' concentration from 2018 to 2021 is mainly associated with the changes in emission patterns.

4.2. Analysis of the Measured Pollutant Concentrations

4.2.1. CO

Figure 4 presents the seasonal variation of CO in the city of São Paulo from 2018 to 2021. From 2020 to 2021, the daily average CO concentration in the summer has progressively decreased, reaching a reduction rate of around −28.0%, varying from (0.63 ± 0.27) ppm observed in 2019 to (0.45 ± 0.15) ppm in 2021. In autumn, a reduction in daily average CO concentration was also observed, which reached (0.46 ± 0.23) ppm in 2020, when the highest

physical distancing rate was registered [25], and (0.50 ± 0.18) ppm in 2021, in comparison with (0.54 ± 0.22) ppm and (0.59 ± 0.21) ppm, observed in 2018 and 2019, respectively. Winter was the season where the higher reduction was registered (around −35.0%), varying from (0.80 ± 0.45) ppm in 2018 to (0.52 ± 0.19) ppm in 2021; regarding spring, 2018, 2019, and 2020 maintained practically the same average values ((0.52 ± 0.17) ppm), and a reduction of around −13.4% could only be observed in 2021, when the concentration reached (0.45 ± 0.14) ppm.

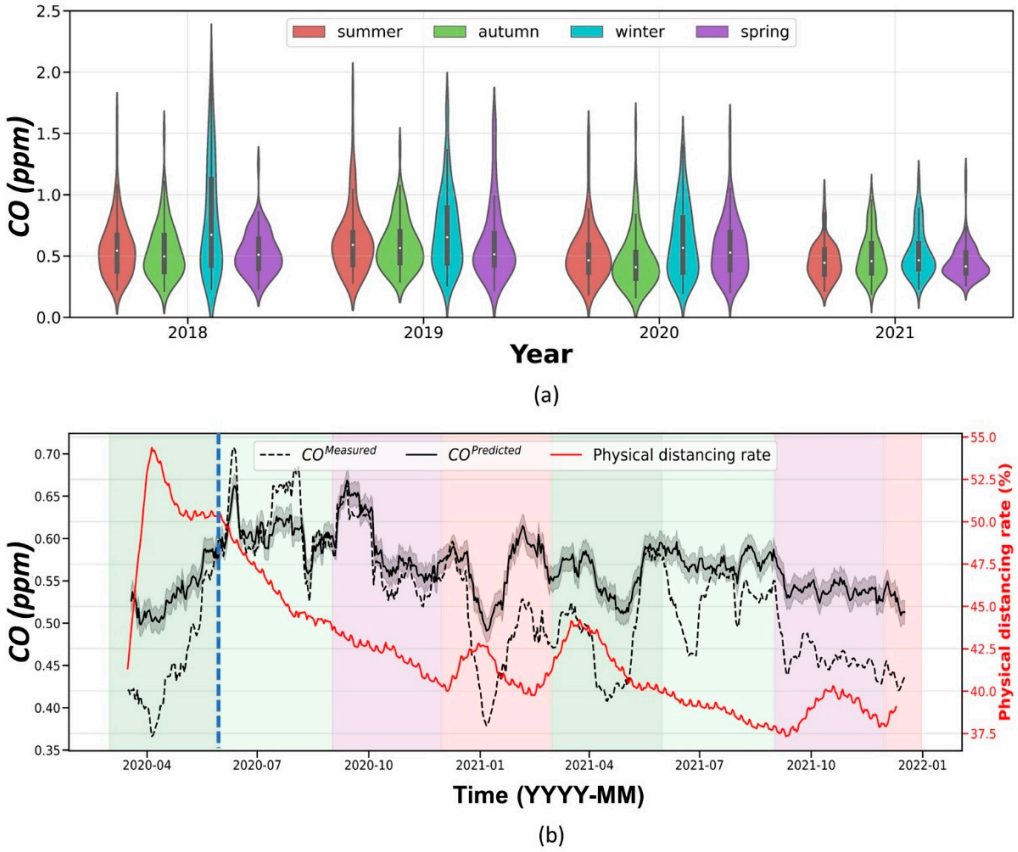

Figure 4. (**a**) Distribution of daily value of CO concentration per season from 2018 to 2021 (1461 cases) in city of São Paulo. (**b**) Comparison among the predicted (black line) and measured (black dotted line) concentrations of CO in city of São Paulo with the physical distancing rate (red line) from March 2020 to December 2021. The black shadow represents the model's mean absolute error. The background green, light green, violet, and red rectangles represent autumn, winter, spring, and summer, respectively. The vertical dotted blue line represents the official day of resumption of economic activities.

Figure 4b compares the measured CO concentrations and the predicted ones from March 2020 to December 2021. During the first weeks of the lockdown, where the physical distancing rate reached higher values (between 55% and 55%), the measured CO concentration (Figure 4b) was lower than predicted. However, as the physical distancing rate decreased, the predicted and measured values became very similar due to the resumption of activities on 1 June 2020. The increase in the physical distancing rate in January (around 42%) and March (about 45%) 2021 obtained a measured CO concentration that was lower than predicted. During the winter of 2021, although the physical distancing rate had decreased, measured CO values were lower than predicted on most days. In the spring of 2021, the new increase in physical distancing rate (reaching around 40%) resulted in lower measured CO concentration values in comparison to the predicted ones.

4.2.2. NO_2

Regarding NO_2 (Figure 5a), a reduction of around −20.4% was observed during the summer; therefore, the concentration ranged from (48.8 ± 16.6) $\mu g \cdot m^{-3}$ in 2019 to (38.8 ± 14.9) $\mu g \cdot m^{-3}$ in 2021. In autumn, although 2020 ((38.0 ± 14.2) $\mu g \cdot m^{-3}$) has a value lower than 2018 ((48.8 ± 15.9) $\mu g \cdot m^{-3}$) and 2019 ((47.0 ± 14.8) $\mu g \cdot m^{-3}$), 2021 presented an increase, reaching (42.8 ± 16.4) $\mu g \cdot m^{-3}$. In the same way as CO, NO_2 has the highest daily average concentrations during winter; hence, the higher variation in NO_2 concentration is observed during this season (−21.7%) due to a reduction from (59.1 ± 21.9) $\mu g \cdot m^{-3}$ in 2018 to (46.3 ± 16.8) $\mu g \cdot m^{-3}$ in 2020. In the spring, as observed in the other seasons, the average values during 2020 and 2021 ((44.7 ± 14.2) $\mu g \cdot m^{-3}$ and (45.4 ± 16.4) $\mu g \cdot m^{-3}$, respectively) are lower than the values measured during 2018 and 2019 ((46.8 ± 13.1) $\mu g \cdot m^{-3}$ and (47.4 ± 18.5) $\mu g \cdot m^{-3}$, respectively).

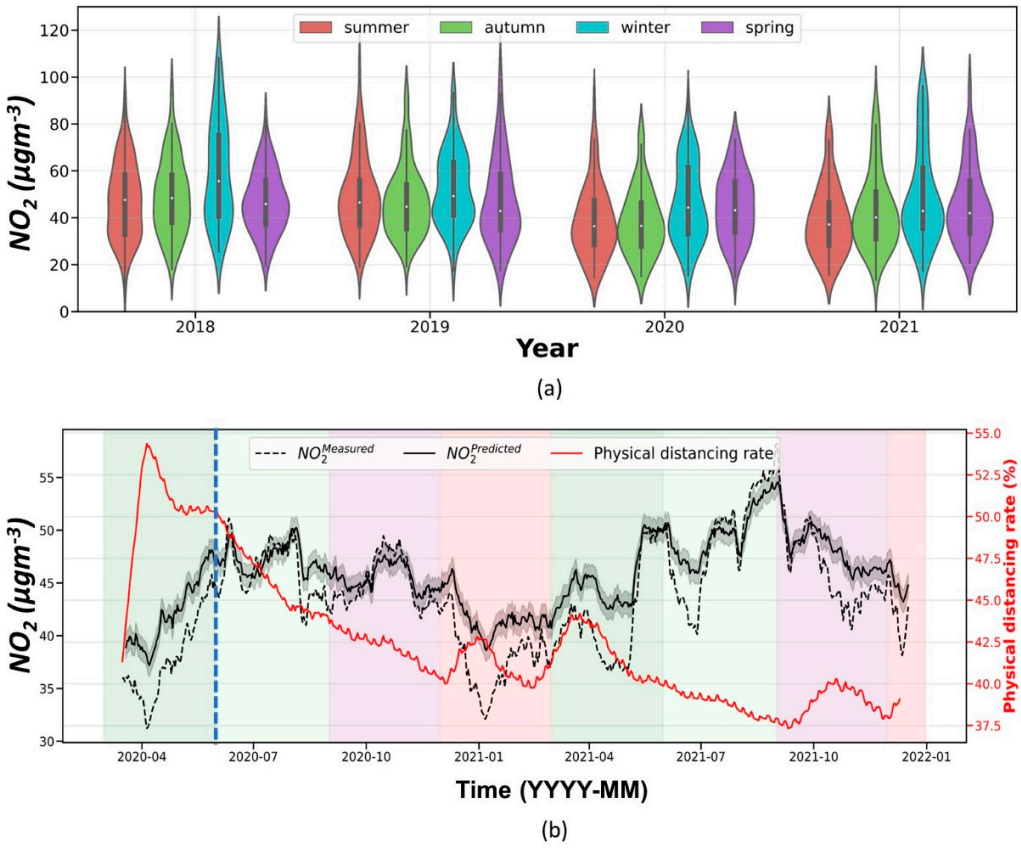

Figure 5. (**a**) Distribution of daily value of NO_2 concentration per season from 2018 to 2021 (1461 cases) in city of São Paulo. (**b**) Comparison among the predicted (black line) and measured (black dotted line) concentrations of NO_2 in city of São Paulo with the physical distancing rate (red line) from March 2020 to December 2021. The black shadow represents the model mean absolute error. The background green, light green, violet, and red rectangles represent autumn, winter, spring, and summer, respectively. The vertical dotted blue line represents the official day of resumption of economic activities.

A comparison between the measured and predicted NO_2 concentrations from March 2020 to December 2021 is presented in Figure 5b. As the physical distancing rate increased (autumn 2020), the measured values became lower than predicted. Therefore, as the physical distancing rate decreased (winter and spring 2020) due to the resumption of activities, measured and predicted values were similar. However, the new increases in the physical distancing rate in January and March 2021 caused lower measured values than predicted. However, the decrease in the physical distancing rate from winter 2021 caused

an increase in the measured NO_2 to reach the predicted values. Winter and autumn 2021 differences are observed when the physical distancing rate is around 40%.

4.2.3. $PM_{2.5}$

The average daily concentration of $PM_{2.5}$ (Figure 6a) presents a reduction of around 9.0% from summer 2019 ((15.9 ± 7.8) $\mu g \cdot m^{-3}$) to summer 2021 ((14.5 ± 5.2) $\mu g \cdot m^{-3}$). During autumn, although 2021 ((16.0 ± 8.0) $\mu g \cdot m^{-3}$) presents an average value above that one registered in 2020 ((15.5 ± 6.6) $\mu g \cdot m^{-3}$), a reduction of 11.0% was observed from 2018 to 2020 (where the average concentration was (17.4 ± 7.7) $\mu g \cdot m^{-3}$). As observed in the previous cases, the winter is the season with the highest (−28.7%) concentration, ranging from (23.7 ± 13.1) $\mu g \cdot m^{-3}$ in 2018 to (16.9 ± 8.3) $\mu g \cdot m^{-3}$ in 2020. However, in the winter of 2021, the $PM_{2.5}$ concentration reached (20.5 ± 13.3) $\mu g \cdot m^{-3}$. Regarding spring, although 2020 and 2021 ((16.9 ± 7.6) $\mu g \cdot m^{-3}$ and (16.4 ± 8.3) $\mu g \cdot m^{-3}$, respectively) had average daily values lower than 2019 ((17.5 ± 9.1) $\mu g \cdot m^{-3}$), both are higher than that one registered in 2018 ((15.4 ± 5.6) $\mu g \cdot m^{-3}$).

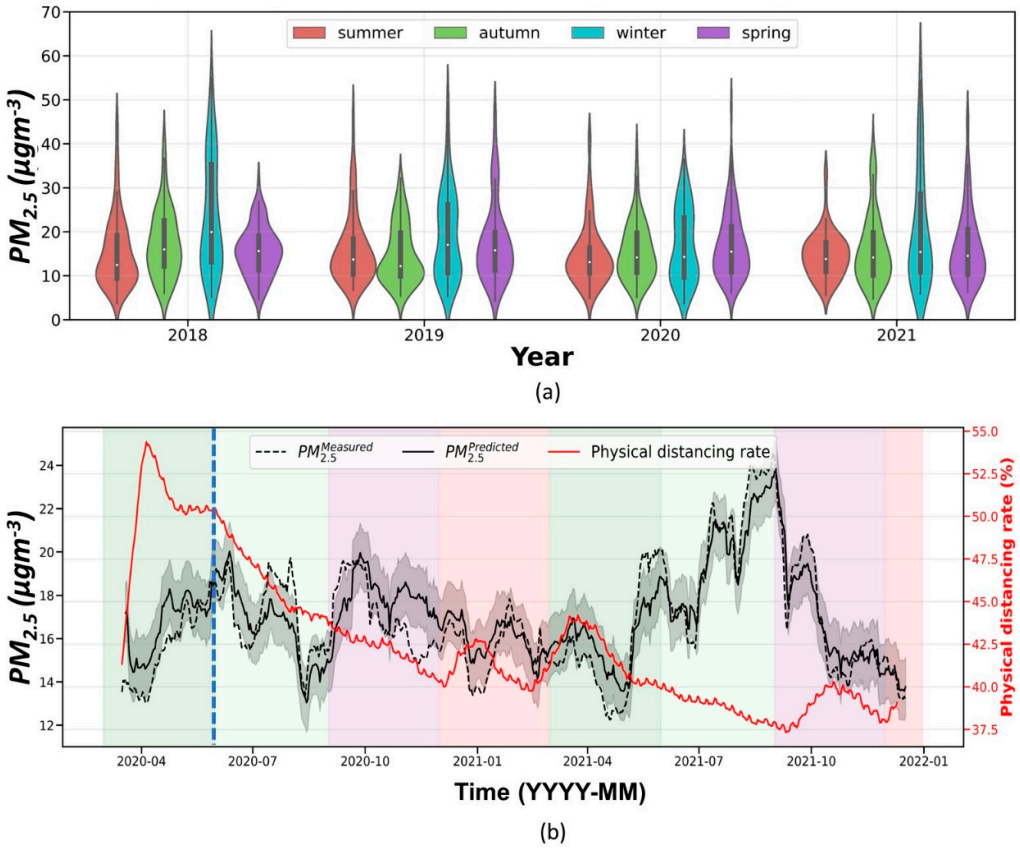

Figure 6. (**a**) Distribution of daily value of $PM_{2.5}$ concentration per season from 2018 to 2021 (1461 cases) in city of São Paulo. (**b**) Comparison among the predicted (black line) and measured (black dotted line) concentrations of $PM_{2.5}$ in city of São Paulo with the physical distancing rate (red line) from March 2020 to December 2021. The black shadow represents the model mean absolute error. The background green, light green, violet, and red rectangles represent autumn, winter, spring, and summer, respectively. The vertical dotted blue line represents the official day of resumption of economic activities.

Opposing what was observed in CO and NO_2 behavior, the measured and predicted $PM_{2.5}$ (Figure 6b) stayed close from March 2020 to December 2021. When there are more significant differences between them, the measured values are contained in the uncertainty region of the model. Moreira et al. [33] demonstrated the relationship between the biomass burning (BB) events in the Brazilian Midwest and the increased $PM_{2.5}$ concentration in the

São Paulo municipality, mainly during autumn and winter. Therefore, the increase in BB events in 2020 and 2021 [34] probably raised the average concentration of $PM_{2.5}$, making a considerable reduction in such pollutants impossible to observe.

4.2.4. PM_{10}

Figure 7 presents the seasonal distribution of the daily average concentration of PM_{10} per season. Regarding the summers, a reduction of 26.5% was observed from 2019 ((27.5 ± 13.2) $\mu g \cdot m^{-3}$) to 2021 ((20.2 ± 8.3) $\mu g \cdot m^{-3}$)). During autumn, although 2021 presents the lowest value ((25.6 ± 13.0) $\mu g \cdot m^{-3}$), 2020 has an average value ((30.5 ± 11.6) $\mu g \cdot m^{-3}$) higher than that one observed in 2018 ((26.4 ± 11.2) $\mu g \cdot m^{-3}$) and 2019 ((28.1 ± 11.9) $\mu g \cdot m^{-3}$). Winter presents a reduction of around 12.9% in the average concentration of PM_{10} from 2018 ((37.3 ± 20.6) $\mu g \cdot m^{-3}$) to 2020 ((32.5 ± 16.1) $\mu g \cdot m^{-3}$). However, in 2021, the concentration rises, reaching (33.9 ± 24.2) $\mu g \cdot m^{-3}$. During spring, a reduction of 14.7% was observed from 2019 ((31.3 ± 14.2) $\mu g \cdot m^{-3}$) to 2021 ((26.7 ± 13.5) $\mu g \cdot m^{-3}$).

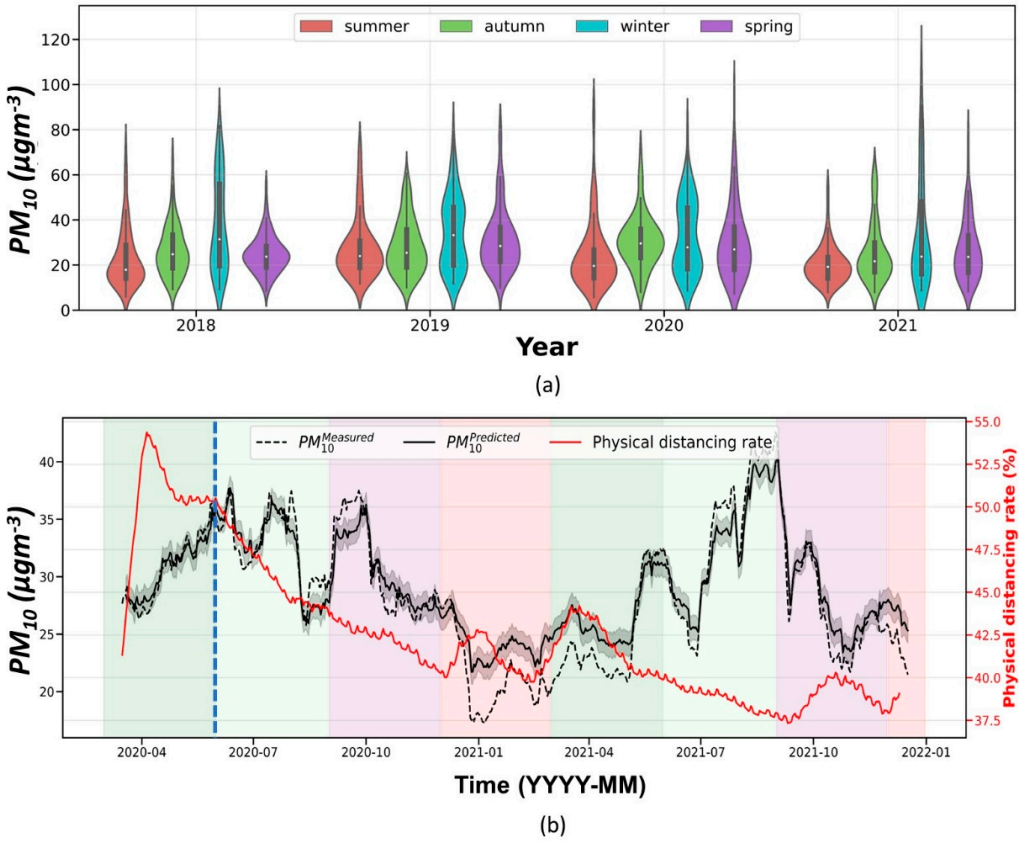

Figure 7. (**a**) Distribution of daily value of PM_{10} concentration per season from 2018 to 2021 (1461 cases) in city of São Paulo. (**b**) Comparison among the predicted (black line) and measured (black dotted line) concentrations of PM_{10} in city of São Paulo with the physical distancing rate (red line) from March 2020 to December 2021. The black shadow represents the model mean absolute error. The background green, light green, violet, and red rectangles represent autumn, winter, spring, and summer, respectively. The vertical dotted blue line represents the official day of resumption of economic activities.

In the same way as $PM_{2.5}$, the measured PM_{10} (Figure 7b) is also poorly influenced by the variations in the physical distancing rate, except in the period between December 2020 and May 2021 (where there was an increase in the physical distancing rate), where predicted PM_{10} is higher than the measured value, and the average PM_{10} concentration observed in the analyzed CETESB stations stays close the values predicted by the model.

5. Discussion

Based on the results presented in the previous section, it is possible to observe that each type of the pollutants that were presented has a particular sensitivity to variations in social distancing, and this is directly associated with the primary source of production of each one.

CO and NO_2 have vehicular traffic as their primary sources of emissions; therefore, it was possible to observe significant changes due to the variance in social isolation. Regarding CO, in which vehicular traffic influences 97% of production [18], insulation values greater than 37% made it possible to observe it in winter, even with unfavorable conditions for the dispersion of pollutants presented in Section 4.1, and lower average concentrations than those recorded in the summer of years without social isolation were observed. The resumption of activities, being partial, did not cause a significant increase in CO concentrations; therefore, especially during spring and summer, when dispersion conditions are more favorable, the observed values remained quite far from the predicted values. On the other hand, NO_2, as it has a smaller percentage of production associated with vehicular traffic (64% for NO_x—[18]), presented a variation that was less sensitive to social distancing rates than CO and was only sensitive when the rates exceeded 41% (it was possible to identify a significant reduction in this way). Although partial, the resumption of activities caused average concentration levels to return to those observed in 2018 and 2019 quickly; thus, the model presented a good correspondence with the values measured when the social distancing rate was below 41%.

PM_{10} and $PM_{2.5}$ do not have vehicular traffic as their primary emission source, contributing only 40% and 37%, respectively. When comparing the variation in average values, the reduction observed was lower than that recorded for CO and NO_2. Thus, the model showed a good correspondence with the measured results, especially for $PM_{2.5}$. The resumption of activities had little influence on both pollutants since the reduction levels observed were within the model's uncertainty margins. Regarding $PM_{2.5}$, it is essential to highlight the increase in the average concentration observed during the autumn and winter of 2021. This characteristic is the consequence of the high number of forest fires registered in the Brazilian central-west and Amazon regions [34], which resulted in several biomass burning episodes in the state of São Paulo [33].

It is essential to highlight that the results presented in this paper are limited to the São Paulo municipality. This methodology can be applied in other regions. However, it is necessary to train the ANN with other time series.

6. Conclusions

In order to demonstrate how the variation in vehicular traffic can affect the concentrations of CO, NO_2, $PM_{2.5}$, and PM_{10} in the city of São Paulo, this paper used the physical distancing caused by the SARS-CoV-2 pandemic to show how the increases or reductions in the vehicle circulation affected the seasonal behaviors of each of these pollutants.

From the meteorological variables analyzed (air surface temperature, relative humidity, accumulated precipitation, and TI position/occurrence), it was possible to conclude that the same seasonal pattern occurred between 2018 and 2021; hence, any event that drastically attenuated or intensified the process of the dispersion of pollutants was recorded. Therefore, summer remained the season with the most significant characteristics to favor the dispersion of pollutants (hot, wet, and with the highest PBLH and VC values). At the same time, winter is endowed with unfavorable characteristics of the dispersion process (cold, dry, lower PBLH and VC values, and higher occurrence of TIs, mainly in the regions above 500 m).

Regarding the concentration of pollutants, those that have vehicular traffic as their main primary source (CO and NO_2) showed a behavior inversely proportional to the rate of physical distancing; therefore, CO is more sensitive to physical distancing than NO_2, reaching average concentration values that were lower than the ones observed in the three previous years during the winter of 2021. On the other hand, the resumption of economic

activities resulted in a fast increase in NO_2; therefore, in 2021, higher values of NO_2 were observed than those in 2018 and 2019.

The pollutants that do not have vehicular traffic as the primary source (PM_{10} and $PM_{2.5}$) showed slight variation concerning the changes in the physical distancing rate, always remaining close to the model and presenting average values similar to the ones observed in 2018 and 2019. Consequently, the resumption of economic activities had a negligible effect on the variations in the concentrations of these pollutants.

From the results of this study, it is possible to observe that the combination of remote sensing instruments, surface data, and machine learning favors the comprehension of pollutant behavior. Furthermore, the results demonstrate that a reduction in vehicular traffic does not directly affect the concentration of pollutants in the same way; hence, the more significant the contribution of vehicular traffic to the primary emission of pollutants, the more intense the effects due to the variations in the physical distancing rate. Therefore, this study reinforces its importance by demonstrating that the relationship between the reduction in vehicular traffic and pollutant concentrations is not a simple question. On the contrary, it is very complex and needs an analysis of several factors because each region has different pollutant sources.

We intend to expand this methodology to other Brazilian urban areas to identify possible differences or similarities in other latitudes, climates, and land covers.

Author Contributions: Conceptualization, G.d.A.M., A.C., A.A.G. and I.d.S.A.; methodology, G.d.A.M. and A.C.; software, G.d.A.M. and A.C.; validation, G.d.A.M., A.C. and I.d.S.A.; formal analysis, G.d.A.M., A.C. and I.d.S.A.; investigation, G.d.A.M., A.C., A.A.G., F.J.d.S.L. and I.d.S.A.; resources, E.L.; data curation, G.d.A.M., A.C. and I.d.S.A.; writing—original draft preparation, G.d.A.M., A.C. and I.d.S.A.; writing—review and editing, G.d.A.M., A.C. and I.d.S.A.; visualization, G.d.A.M., A.C. and I.d.S.A.; supervision, E.L.; funding acquisition, E.L. All authors have read and agreed to the published version of the manuscript.

Funding: This research was funded by the National Council for Scientific and Technological Development (CNPq) (project 432515/2018-6), Coordination for the Improvement of Higher Education Personnel (CAPES) (scholarships: 88887.464990/2019-00, PROEX 88887.595780/2020-00).

Institutional Review Board Statement: Not applicable.

Informed Consent Statement: Informed consent was obtained from all subjects involved in this study.

Data Availability Statement: The data presented in this study are available upon request from the corresponding author.

Acknowledgments: The authors thank the São Paulo State CETESB for providing the data through the QUALAR database and the INMET for the data about the rainfall rates.

Conflicts of Interest: The authors declare no conflict of interest.

References

1. Sokhi, R.S.; Moussiopoulos, N.; Baklanov, A.; Bartzis, J.; Coll, I.; Finardi, S.; Friedrich, R.; Geels, C.; Grönholm, T.; Halenka, T.; et al. Advances in air quality research—Current and emerging challenges. *Atmos. Chem. Phys.* **2022**, *22*, 4615–4703. [CrossRef]
2. Manisalidis, I.; Stavropoulou, E.; Stavropoulos, A.; Bezirtzoglou, E. Environmental and Health Impacts of Air Pollution: A Review. *Front. Public Health* **2020**, *8*, 14. [CrossRef]
3. Adam, M.G.; Tran, P.T.M.; Balasubramanian, R. Air quality changes in cities during the COVID-19 lockdown: A critical review. *Atmos. Res.* **2021**, *264*, 105823. [CrossRef] [PubMed]
4. Ścisło, Ł.; Łacny, Ł.; Guinchard, M. COVID-19 lockdown impact on CERN seismic station ambient noise levels. *Open Eng.* **2021**, *11*, 1233–1240. [CrossRef]
5. Caniato, M.; Bettarello, F.; Gasparella, A. Indoor and outdoor noise changes due to the COVID-19 lockdown and their effects on individuals' expectations and preferences. *Sci. Rep.* **2021**, *11*, 16533. [CrossRef]
6. Li, C.; Li, X.; Zhu, C. Night-Time Skyglow Dynamics during the COVID-19 Epidemic in Guangbutun Region of Wuhan City. *Remote Sens.* **2022**, *14*, 4451. [CrossRef]

7. Silva, A.C.T.; Branco, P.T.B.S.; Sousa, S.I.V. Impact of COVID-19 Pandemic on Air Quality: A Systematic Review. *Int. J. Environ. Res. Public Health* **2022**, *19*, 1950. [CrossRef]
8. Dantas, G.; Siciliano, B.; França, B.; da Silva, C.M.; Arbilla, G. The impact of COVID-19 partial lockdown on the air quality of the city of Rio de Janeiro, Brazil. *Sci. Total Environ.* **2020**, *729*, 139085. [CrossRef]
9. Moreira, G.A.; Andrade, I.S.; Cacheffo, A.; Yoshida, A.C.; Gomes, A.A.; Silva, J.J.; Lopes, F.J.S.; Landulfo, E. COVID-19 outbreak and air quality: Analyzing the influence of physical distancing and the resumption of activities in São Paulo municipality. *Urban. Clim.* **2021**, *37*, 100813. [CrossRef]
10. Wang, P.; Chen, K.; Zhu, S.; Wang, P.; Zhang, H. Severe air pollution events not avoided by reduced anthropogenic activities during the COVID-19 outbreak. *Resour. Conserv. Recycl.* **2020**, *158*, 104814. [CrossRef]
11. Zalakeviciute, R.; Vasquez, R.; Bayas, D.; Buenano, A.; Mejia, D.; Zegarra, R.; Diaz, A.; Lamb, B. Drastic Improvements in Air Quality in Ecuador during the COVID-19 Outbreak. *Aerosol Air Qual. Res.* **2020**, *20*, 1783–1792. [CrossRef]
12. Sharma, S.; Zhang, M.; Gao, J.; Zhang, H.; Kota, S.H. Effect of restricted emissions during COVID-19 on air quality in India. *Sci. Total Environ.* **2020**, *728*, 138878. [CrossRef] [PubMed]
13. Collivignarelli, M.C.; Abbà, A.; Bertanza, G.; Pedrazzani, R.; Ricciardi, P.; Miino, M.C. Lockdown for COVID-2019 in Milan: What are the effects on air quality? *Sci. Total Environ.* **2020**, *732*, 139280. [CrossRef] [PubMed]
14. Otmani, A.; Benchrif, A.; Tahri, M.; Bounakhla, M.; Chakir, E.M.; Bouch, M.E.; Krombi, E. Impact of Covid-19 lockdown on PM_{10}, SO_2, and NO_2 concentrations in Salé City (Morocco). *Sci. Total Environ.* **2020**, *735*, 139541. [CrossRef] [PubMed]
15. Sicard, P.; De Marco, A.; Agathokleous, E.; Feng, Z.; Xu, X.; Paoletti, E.; Rodriguez, J.J.D.; Calatayud, V. Amplified ozone pollution in cities during the COVID-19 lockdown. *Sci. Total Environ.* **2020**, *735*, 139542. [CrossRef] [PubMed]
16. Bekbulat, B.; Apte, J.S.; Millet, D.B.; Robinson, A.L.; Wells, K.C.; Presto, A.A.; Marshall, J.D. Changes in criteria air pollution levels in the US before, during, and after Covid-19 stay-at-home orders: Evidence from regulatory monitors. *Sci. Total Environ.* **2021**, *769*, 144693. [CrossRef]
17. IBGE. Instituto Brasileiro de Geografia e Estatística. 2022. Available online: http://ibge.gov.br (accessed on 1 January 2022).
18. Andrade, M.F.; Kumar, P.; Freitas, E.D.; Ynoue, R.Y.; Martins, J.; Martins, L.D.; Nogueira, T.; Perez-Martinez, P.; Miranda, R.M.; Albuquerque, T.; et al. Air quality in the megacity of São Paulo: Evolution over the last 30 years and future perspectives. *Atmos. Environ.* **2017**, *159*, 66–82. [CrossRef]
19. CETESB. Qualidade do Ar no Estado de São Paulo 2018. 2019. Available online: https://cetesb.sp.gov.br/ar/wp-content/uploads/sites/28/2019/07/Relat%C3%B3rio-de-Qualidade-do-Ar-2018.pdf (accessed on 1 June 2021).
20. São Paulo Municipality. 2022. Available online: https://www.prefeitura.sp.gov.br/ (accessed on 1 January 2022).
21. Siciliano, B.; Carvalho, G.; da Silva, C.M.; Arbilla, G. The Impact of COVID-19 Partial Lockdown on Primary Pollutant Concentrations in the Atmosphere of Rio de Janeiro and São Paulo Megacities (Brazil). *Bull. Environ. Contam. Toxicol.* **2020**, *105*, 2–8. [CrossRef]
22. Nakada, L.Y.K.; Urban, R.C. COVID-19 pandemic: Impacts on the air quality during the partial lockdown in São Paulo state, Brazil. *Sci. Total Environ.* **2020**, *730*, 139087. [CrossRef]
23. Moreira, G.A.; Oliveira, A.P.; Sánchez, M.P.; Codato, G.; Lopes, F.J.S.; Landulfo, E.; Filho, E.P.M. Performance assessment of aerosol-lidar remote sensing skills to retrieve the time evolution of the urban boundary layer height in the Metropolitan Region of São Paulo City, Brazil. *Atmos. Res.* **2022**, *277*, 106290. [CrossRef]
24. CETESB. Padrões de Qualidade do Ar. 2020. Available online: https://cetesb.sp.gov.br/ar/padroes-de-qualidade-do-ar/ (accessed on 10 June 2021).
25. Assembleia Legislativa do Estado de São Paulo. *Decreto Nº 59.113, de 23 de Abril de 2013. Estabelece Novos Padrões de Qualidade do ar e dá Providências Correlatas*; Assembleia Legislativa: São Paulo, Brazil, 2013. Available online: https://cetesb.sp.gov.br/qualidade-ar/wp-content/uploads/sites/28/2013/12/decreto-59113de230413.pdf (accessed on 1 January 2022).
26. Moreira, G.A.; Lopes, F.J.S.; Guerrero-Rascado, J.L.; Silva, J.J.; Gomes, A.A.; Landulfo, E.; Alados-Arboledas, L. Analyzing the atmospheric boundary layer using high-order moments obtained from multiwavelength lidar data: Impact of wavelength choice. *Atmos. Meas. Tech.* **2019**, *12*, 4261–4276. [CrossRef]
27. INMET. Instituto Nacional de Meteorologia. 2020. Available online: http://www.inmet.gov.br/ (accessed on 1 January 2022).
28. CETESB. Qualidade do ar (QUALAR). 2023. Available online: https://cetesb.sp.gov.br/ar/qualar/ (accessed on 4 August 2023).
29. Stull, R.B. *An Introduction to Boundary Layer Meteorology*; Springer: Dordrecht, The Netherlands, 1988.
30. Granados-Muñoz, M.J.; Navas-Guzmán, F.; Bravo-Aranda, J.A.; Guerrero-Rascado, J.L.; Lyamani, H.; Fernández-Gálvez, J.; Alados-Arboledas, L. Automatic determination of the planetary boundary layer height using lidar: One-year analysis over southeastern Spain. *J. Geophys. Res.* **2012**, *117*, D18208. [CrossRef]
31. Moreira, G.A.; Guerrero-Rascado, J.L.; Bravo-Aranda, J.A.; Foyo-Moreno, I.; Cazorla, A.; Alados, I.; Lyamani, H.; Landulfo, E.; Alados-Arboledas, L. Study of the planetary boundary layer height in an urban environment using a combination of microwave radiometer and ceilometer. *Atmos. Res.* **2020**, *240*, 104932. [CrossRef]
32. Triebe, O.; Hewamalage, H.; Pilyugina, P.; Laptev, N.; Bergmeir, C.; Rajagopal, R. NeuralProphet: Explainable Forecasting at Scale. *arXiv* **2021**, arXiv:2111.15397. [CrossRef]

33. Moreira, G.A.; da Silva Andrade, I.; Cacheffo, A.; da Silva Lopes, F.J.; Calzavara Yoshida, A.; Gomes, A.A.; da Silva, J.J.; Landulfo, E. Influence of a Biomass-Burning Event in PM2.5 Concentration and Air Quality: A Case Study in the Metropolitan Area of São Paulo. *Sensors* **2021**, *21*, 425. [CrossRef]
34. Pivello, V.R.; Vieira, I.; Christianini, A.V.; Ribeiro, D.B.; Menezes, L.S.; Berlinck, C.N.; Melo, F.P.L.; Marengo, J.A.; Tornquist, C.G.; Tomas, W.M.; et al. Understanding Brazil's catastrophic fires: Causes, consequences and policy needed to prevent future tragedies. *Perspect. Ecol. Conserv.* **2021**, *19*, 3. [CrossRef]